THE ASTROPHYSICAL JOURNAL, 436:L31–L34, 1994 November 20

RAPID X-RAY SPECTRAL VARIABILITY IN NGC 3227

A. PTAK,[1] T. YAQOOB,[2] P. J. SERLEMITSOS, AND R. MUSHOTZKY
NASA/Goddard Space Flight Center, Greenbelt, MD 20771

AND

C. OTANI
Institute of Space and Astronautical Science, Yoshinodai, Sagamihara, Kanagawa 229, Japan
Received 1994 June 3; accepted 1994 August 28

ABSTRACT

We present preliminary results of an *ASCA* observation of the Seyfert 1 galaxy, NGC 3227. The source exhibits rapid X-ray amplitude and spectral variability, the flux below 2 keV varying by a factor of ~ 3 in $\sim 10{,}000$ s while the flux in the 2–10 keV band varies by a factor of ~ 2 in the same interval. The spectrum below ~ 1 keV shows complex structure compared to a simple power-law model. We argue that the simplest interpretation of the spectrum is in terms of a power-law continuum modified by absorption in a photoionized medium. Simple, static, ionized absorber models yield an ionization parameter of ~ 0.05 and column density $\sim 3.6 \times 10^{21}$ cm^{-2}. However, the data strongly indicate that the situation is much more complex than this. If the spectral variability is caused by a changing ionization state of the absorber, then both the ionization state and column density are required to decrease as the intrinsic source luminosity increases. This does not have a simple physical interpretation. On the other hand, the data are also consistent with the spectral variability being due to changes in the intrinsic power-law index with little change in the ionization state of the absorber. This case could correspond to an absorber which is always in some average ionization state and the continuum variability is too fast for the absorber to deviate significantly from that, or the absorber could be in the form of an X-ray–heated wind.

Subject headings: galaxies: individual (NGC 3227) — galaxies: Seyfert — X-rays: galaxies

1. INTRODUCTION

Two very important X-ray diagnostics of active galactic nuclei (AGNs) are (1) complex spectral features and (2) spectral variability. Recent data point to similar, prominent absorption structures below ~ 1 keV or so in several AGNs which are thought to be signatures of a photoionized medium in the line of sight (e.g., Nandra & Pounds 1992; Turner et al. 1993; Fabian et al. 1994). The location and physical structure of this so-called "warm absorber" is, as yet, not well understood. Work in obtaining precise measurements of the parameters of the putative warm absorber has only just begun since it demands the good energy resolution, broad bandpass, and high sensitivity of *ASCA*. If we can measure its distance from the central engine, its density, temperature, and size, we can begin to assess its role as a component of models of the active nucleus.

The other diagnostic, spectral variability, has been reported for several AGNs on timescales of ~ 1 day or greater. These tend to be objects which have been frequently monitored, notable examples being NGC 5548 (Nandra et al. 1991), NGC 4151 (Yaqoob et al. 1993) and MGC -6-30-15 (Fabian et al. 1994). Depending on the individual case, spectral variability can provide invaluable information on the X-ray emission mechanism, changing ionization state and/or configuration of X-ray–absorbing material in the nucleus, or reprocessing of the primary X-ray emission. In some cases spectral variability may be due to the differential variability of two emission components. Conclusive evidence of *rapid* spectral variability on timescales of less than 1 day is much scarcer (a notable example is NGC 4051; Matsuoka et al. 1990). However, the reduced statistics of time-resolved spectra has made it difficult to reach any unambiguous conclusions about the origin of the rapid spectral variability when it has been observed.

NGC 3227 ($z = 0.003$) is a variable low-luminosity Seyfert 1 galaxy with a 2–10 keV intrinsic luminosity measured by *EXOSAT* (Turner & Pounds 1989) and *Ginga* (George, Nandra, & Fabian 1990) in the range $\sim (0.5\text{–}2.1) \times 10^{42}$ ergs s^{-1} ($H_0 = 50$ km s^{-1} Mpc^{-1} and $q_0 = 0$ throughout this *Letter*). A series of five *EXOSAT* observations over a period of ~ 8 months found the ratio of soft flux (~ 0.1–1 keV) measured by the Low Energy Telescope (LE) to the hard flux (~ 2–10 keV) measured by the Medium Energy experiment (ME) to be variable by a factor ~ 5 among the set of observations which had a minimum separation of 7 days (Turner & Pounds 1989). However, the LE had no spectral resolution and the ME had no sensitivity below ~ 1–2 keV so the origin of the spectral variability remained unknown.

2. THE *ASCA* DATA

NGC 3227 was observed by *ASCA* (SIS in 4-CCD mode) on 1993 May 8. See Tanaka, Holt, & Inoue (1994) for a summary of the *ASCA* mission and focal-plane detectors. Hereafter, the two SIS sensors are referred to as SIS0 and SIS1 and the two GIS sensors as GIS2 and GIS3. Data reduction procedures closely follow those in Serlemitsos et al. (1994). Extracted total count rates for spectra from the four instruments ranged from ~ 0.5 to 0.8 counts s^{-1} and the background constitutes $\sim 1\%$–3% of the total in the SIS and $\sim 2\%$–3% of the total in the GIS. In the following analysis, all spectra were binned so that there was a minimum of 20 counts per energy bin. This allows us to use the χ^2 minimization technique in the spectral fitting process. Also, since we will be most interested in spectral

[1] University of Maryland, College Park MD 20742.
[2] With the Universities Space Research Association.

features below 2 keV in this *Letter*, we will concentrate mainly on data for SIS0. The remaining three instruments will be used for confirming results and tightening constraints on the continuum. SIS0 is better calibrated below ~2 keV at the present, and there were twice as many counts in SIS0 as in SIS1—owing to the location of the source relative to the optical axes and CCD gaps. Note that since the source is relatively bright, the binning only affects data above 3.6 keV and does not "wash out" spectral features below this energy.

3. AMPLITUDE AND SPECTRAL VARIABILITY

Figure 1 (*top*) shows the 0.4–10.0 keV light curve for SIS0 from which dramatic amplitude variability is clearly evident. The points in the light curve were computed from the count rates in the final, merged good time intervals after data selection, so the bin size is variable, varying from ~300 to 2200 s. Using small fixed bins sizes gives poor statistics while large bin sizes can "wash out" variability. The largest amplitude change corresponds to an increase of almost a factor of 2 in ~10,000 s (the second peak in the light curve). The next two panels in Figure 1 show light curves for SIS0, in the energy bands 0.4–2 keV and 2–10 keV, respectively. The 0.4–2 keV band count rate varies by almost a factor of 3 in ~10,000 s, while the 2–10 keV band count rate varies by a factor of 2 in the same interval. Figure 1 (*bottom*) shows, for SIS0, the ratio of the 0.4–2 keV to 2–10 keV count rates (after background subtraction) versus time and confirms the rapid spectral variability apparent from the individual light curves in the two central panels in Figure 1. The hypothesis of a constant softness ratio in Figure 1 (*bottom*) results in a χ^2 of 59.6 for 33 d.o.f., unacceptable at a level of 99.7%. The same pattern in both amplitude and spectral variability is observed in the light curves for SIS1 to GIS3.

We extracted two spectra from the SIS0 data—one when the 0.4–10 keV count rate was between 0 and 0.6 counts s^{-1} (hereafter the "low-state" spectrum) and the other greater than 0.7 counts s^{-1} (hereafter the "high-state" spectrum). The same time intervals used to extract the SIS0 low- and high-state spectra were then applied to data from SIS1 to GIS3 to extract three more pairs of low- and high-state spectra. Fitting the ratios of the high-state spectra to the low-state spectra for SIS0 to GIS3 with a constant gives values of χ^2 which are unacceptable at levels of 99.8%, 83.1%, 95.9% for SIS0, SIS1, and GIS3 respectively; however, the fit for GIS3 is acceptable with a reduced χ^2 of 0.9. There may be some mixing between the low- and high-state spectra due to statistical fluctuations in the count rate, which would tend to move the results to the constant ratio hypothesis (this effect was also seen when high- and low-state spectra were selected in SIS0 using softness rather than intensity as the selection criterion due to the larger error bars in the softness ratio). Fitting the spectral ratios with a power law gives acceptable fits for all instruments, consistent with a spectral index change of ~ +0.2 between the low and high states.

4. SPECTRAL FITTING

For either the low- or high-state SIS spectra, a simple power-law model with cold, uniform, solar abundance absorption provides an unacceptable fit, leaving broad structures in the residuals. This can be seen in Figure 2 which shows the ratios of data to model for the SIS0 low- and high-state spectra. Evidence for spectral complexity at low energies was in fact suggested by an off-axis *ROSAT* PSPC observation of NGC 3227 (T. J. Turner, private communication). Also evident

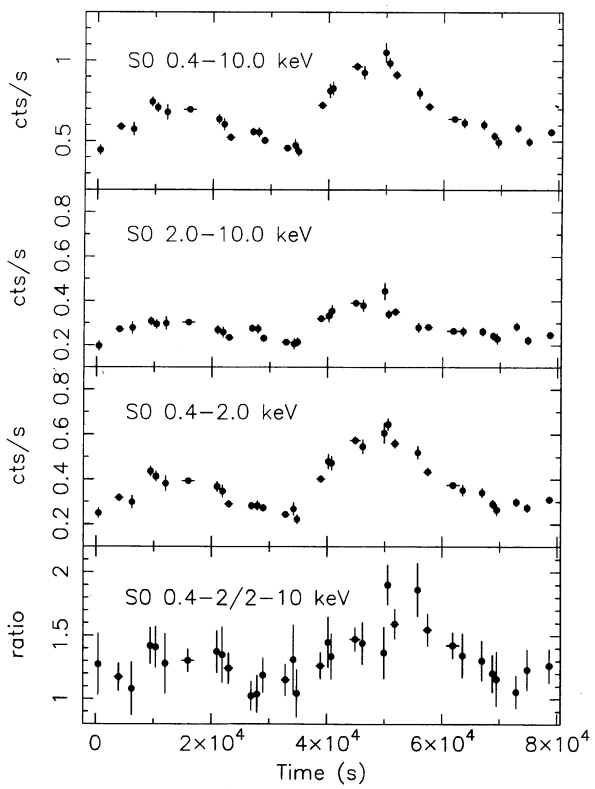

FIG. 1.—*Top:* The 0.4–10.0 keV light curve from SIS0. *Bottom:* Ratio of 0.4–2 keV to 2–10 keV count rates for SIS0.

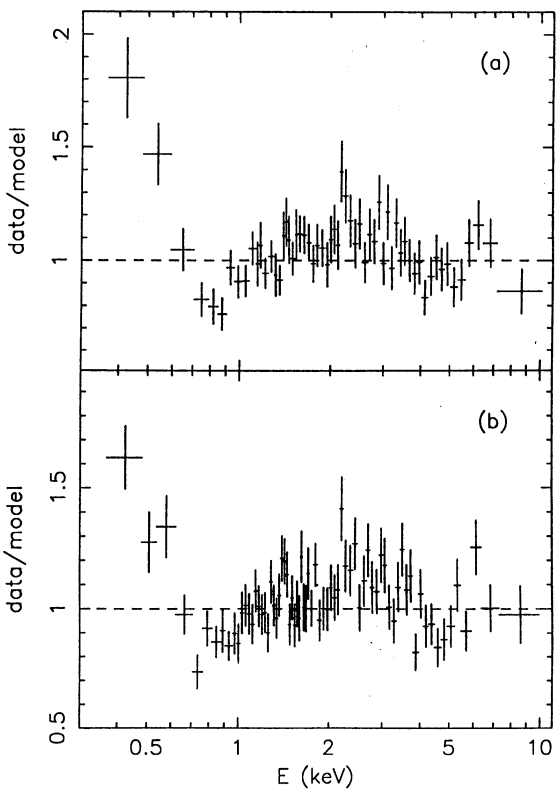

FIG. 2.—Ratio of SIS0 data to simple power-law plus cold absorber model for (*a*) the low state and (*b*) the high state.

in Figure 2 is a prominent Fe Kα emission-line feature between 6 and 7 keV, discovered by *Ginga* (Pounds et al. 1989; George et al. 1990). In all the spectral fitting described below, we include it in the models as a Gaussian component whose center energy, intrinsic width, and normalization are free parameters. Also, unless otherwise stated all errors correspond to a 90% confidence interval for two interesting parameters.

In a preliminary spectral fitting analysis, we tried modeling the complex soft X-ray spectrum by adding to the simple power-law plus absorber model (*a*) another power law, (*b*) a blackbody, and (*c*) an absorption edge with optical depth $\tau = \tau_0(E/E_0)^{-3}$. All three model components involve the addition of two free parameters and can qualitatively account for the complexity at low energies. The χ^2 values of these fits and others discussed below are shown in Table 1. The power-law plus blackbody provides a better fit for the high state than the double power law although the low-state SIS0 spectrum can be fitted equally well by both models. The power-law plus absorption-edge model provides a better fit to both the low and high states (compared to the power-law plus blackbody model). For both high and low states, the threshold energy and optical depth of the edge are $E_0 \sim 0.7$ keV and $\tau_0 \sim 0.7$. The two-component continuum models leave significant residuals below $\sim$0.7 keV which can be modeled by an absorption edge with the same parameters as above (or an emission line, as shown in Table 1). We caution that the precise parameters for the absorption edge should be interpreted with care because there are remaining systematics near the oxygen edge in the SIS response, of the order of $\sim$5%–10%. However, those residuals are qualitatively different than the ones we are discussing in NGC 3227 and are much smaller (see Yaqoob et al. 1994).

Since the two-component continuum models still require an additional low-energy feature and a simpler, one-component continuum with a similar feature can describe the data equally well, we do not consider two-component continuum models any further. Returning to the power-law plus absorption-edge model, we find that adding another absorption edge is marginally significant (at levels of 97% and 89% for the low and high state, respectively). The results of this fit are shown in Table 2. The data, best-fitting model, and ratios of data to model are shown in Figure 3. The best-fitting column densities are a factor 2–3 higher than the Galactic value of 0.36×10^{21} cm^{-2} (Stark et al. 1992). The best-fitting values of the edge parameters E_1 and τ_1 are remarkably similar in the low and high states with $E_1 \sim 0.67$ keV and $\tau_1 \sim 0.75$ for both spectra. This edge can be interpreted as being due predominantly to O VI, but its energy is also consistent with N VII. The second edge is likely to be predominantly due to O VII–O VIII, although its statistical significance is not high. In passing we note that the Fe K line appears to be broader in the low state. However, this requires further detailed investigation which will be reported in future work. Also, note the rather high value of χ^2 for the high-state fit, despite the good overall fit. The largest contribution to χ^2 comes from a local feature at $\sim$4 keV, which when modeled as a notch, reduces χ^2 by 16.6 (two additional parameters). The origin of this feature is unknown (it is not present in SIS1). Table 2 shows that the photon index, Γ, for the low state is lower than that for the high state, by $\sim$0.2, as expected from the spectral ratios. The 90% confidence ranges exclude a single value of Γ. We tightened the constraints on Γ further by repeating the fits using data from all four instruments simultaneously, and this gives $\Gamma = 1.52^{+0.02}_{-0.06}$ for the low state and $\Gamma = 1.65^{+0.04}_{-0.03}$ for the high state.

TABLE 1

χ^2 VALUES FOR VARIOUS FITS TO SIS0 DATA

Model	Low State	High State
Power law	224.6(169)	271.9(167)
Two power laws	162.0(167)	215.8(165)
Two power laws + Gaussian	143.9(164)	191.1(162)
Power law + blackbody	162.5(167)	208.2(165)
Power law + blackbody + Gaussian	146.8(164)	190.5(162)
Power law + edge	154.4(167)	197.7(165)
Power law + two edges	146.0(165)	193.3(163)

NOTE.—Parentheses indicate the number of degrees of freedom. All models include a cold absorber and an Fe K emission line (see text).

TABLE 2

POWER-LAW PLUS ABSORPTION-EDGE FITS TO SIS0

Parameter	Low State	High State
Γ	1.46 (1.37–1.55)	1.67 (1.59–1.76)
N_H (10^{21} cm^{-2})	0.88 (0.62–1.20)	1.02 (0.83–1.33)
Edge E_1 (keV)	0.66 (0.61–0.69)	0.67 (0.63–0.70)
Edge τ_1	0.74 (0.35–1.07)	0.76 (0.52–1.00)
Edge E_2 (keV)	0.81 (0.72–1.03)	0.90[a]
Edge τ_2	0.32 (0.06–0.65)	<0.32[b]
Fe K E (keV)	6.38 (6.05–6.76)	6.42 (6.33–6.51)
Fe K σ (keV)	0.32 (0.07–0.81)	0.085 (0.00–0.28)
Fe K EW (eV)	296 (79–508)	259 (115–404)
χ^2 (d.o.f.)	146.0 (165)	193.3 (163)

NOTE.—Parentheses indicate 90% confidence intervals for two interesting parameters.

[a] Errors not quoted, as this edge is only marginally significant.

[b] Upper limit for $\Delta\chi^2 = 4.61$.

We measure the ratio of observed flux in the high state to that in the low state to be 1.9 and 1.4 in the 0.4–2 keV and 2–10 keV bands, respectively. The corresponding absorption-corrected ratios differ by no more than 5%. Absolute SIS fluxes are at present subject to uncertainties in exposure corrections. However, we estimate the mean 2–10 keV observed flux from GIS2 and GIS3 over the entire observation to be $\sim 2.5 \times 10^{-11}$ ergs cm^{-2} s^{-1}, corresponding to a 2–10 keV absorption-corrected luminosity of $\sim 1.0 \times 10^{42}$ ergs s^{-1}.

5. WARM ABSORBER

Naturally, the above results suggest an interpretation in terms of the X-ray spectrum being modified by a photoionized absorber in the line of sight, which might also explain the apparent change in Γ due to the broader opacity profile of an ionized absorber compared to a neutral one. We therefore fitted the SIS0 data with a power-law plus simple warm-absorber model (as in Yaqoob & Warwick 1991), also including an additional cold absorber. In all of the following fits, the best-fitting column density of the cold absorber is always consistent with the Galactic value. Unfortunately, individual fits to the low- and high-state data give ambiguous results due to the complex interaction of Γ, the ionization parameter (U), and the column density of the warm absorber (N_w). However, we can repose the problem in two ways: can the low and high states be fitted simultaneously with (1) the same value of Γ, and (2) the same value of U and N_w? Excellent fits are obtained for *both* cases, giving $\chi^2 = 347.8$ (334 d.o.f.) for case (1) and $\chi^2 = 344.6$ (335 d.o.f.) for case (2). However, for case (1), from the low to

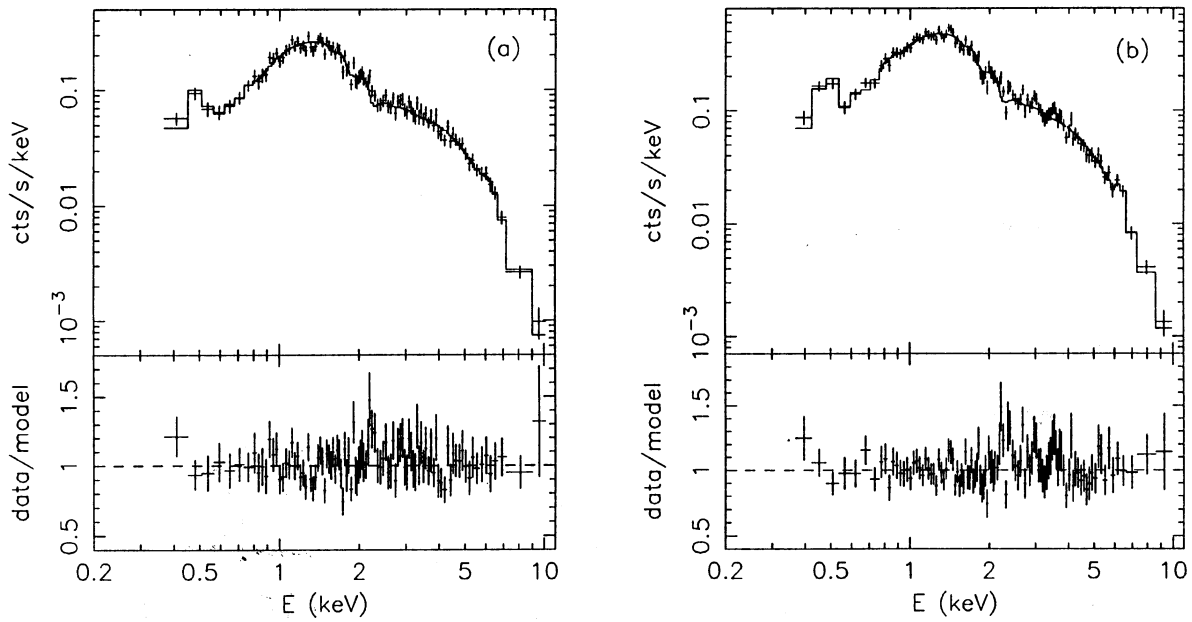

FIG. 3.—SIS0 data, best-fitting power-law plus absorption-edge models for (*a*) the low state and (*b*) the high state. The residuals at 2.1 keV are due to a known artifact in the SIS response.

high states, log U decreases from $-1.17^{+0.11}_{-0.18}$ to $-1.43^{+0.17}_{-0.16}$, and log N_w decreases from $21.72^{+0.06}_{-0.10}$ to $21.42^{+0.11}_{-0.11}$. This raises the question as to why N_w should decrease in response to an increase in the luminosity and suggests that the model may be too simple. For case (2) we get best-fitting parameters log $U = -1.35^{+0.12}_{-0.14}$, log $N_w = 21.56^{+0.13}_{-0.12}$, $\Gamma = 1.49^{+0.06}_{-0.07}$ for the low state and $\Gamma = 1.75^{+0.07}_{-0.08}$ for the high state (when U is not held at the same value the best-fitting values of U are still log $U \sim -1.3$ for both states). Case (2), which corresponds to the spectral variability being caused by intrinsic power-law index changes with little change in the ionization state of the absorber, again indicates that the simple warm-absorber model is inadequate. This is because for the given change in spectrum and luminosity between the low and high states, and for a fixed gas density of the absorber and its distance from the central source, we estimate that the ionization parameter should increase by a factor of ~ 1.7. The real situation may be one in which the absorber is always in some average state of ionization due to the time required to adjust in the continuum being much longer than the variability timescale of the ionizing continuum. Alternatively, the absorber may be in the form of an X-ray–heated wind, in which the density scales as r^{-2} and the ionization parameter is "frozen in." Detailed interpretation of these results will be discussed in future work.

The authors wish to thank all the members of the *ASCA* team who have made this work possible. A. P., T. Y., P. J. S., and R. M. thank the Institute of Space and Astronautical Science (ISAS) for their hospitality during the summer of 1993 where part of this work was done.

REFERENCES

Fabian, A. C., et al. 1994, PASJ, 46, L59
George, I. M., Nandra, K., & Fabian, A. C. 1990, MNRAS, 242, 28P
Matsuoka, M., Piro, L., Yamauchi, M., & Murakami, T. 1990, ApJ, 361, 440
Nandra, K., & Pounds, K. A. 1992, Nature, 359, 215
Nandra, K., Pounds, K. A., Stewart, G. C., George, I. M., Hayashida, K., Makino, F., & Ohashi, T. 1991, MNRAS, 248, 760
Pounds, K. A., Nandra, K., Stewart, G. C., & Leighly, K. 1989, MNRAS, 240, 769
Serlemitsos, P. J., et al. 1994, PASJ, 46, L43
Stark, A. A., Gammie, C. F., Wilson, R. W., Bally, J., Linke, R., Heiles, C., & Hurwitz, M. 1992, ApJS, 79, 77
Tanaka, Y., Holt, S. S., & Inoue, H. 1994, PASJ, 46, L37
Turner, T. J., Nandra, K., George, I. M., Fabian, A. C., & Pounds, K. A. 1993, ApJ, 419, 127
Turner, T. J., & Pounds, K. A. 1989, MNRAS, 240, 833
Yaqoob, T., et al. 1994, PASJ, 46, L49
Yaqoob, T., & Warwick, R. S. 1991, MNRAS, 248, 773
Yaqoob, T., Warwick, R. S., Makino, F., Otani, Y., Sokoloski, J. L., Yamauchi, M., & Bond, I. A. 1993, MNRAS, 262, 435